Journal of Simulation and Analysis of Novel Technologies in Mechanical Engineering
13 (1) (2021) 0043~0053
HTTP://JSME.IAUKHSH.AC.IR

Research article

Analysis of airflow on an airfoil using electro-hydrodynamic actuators

Mohammad Bigdeli, Alireza Ansari, Gholamreza Tathiri, Vahid Monfared*

Department of Mechanical Engineering, Zanjan Branch, Islamic Azad University, Zanjan, Iran

*vahid_monfared@alum.sharif.edu

(Manuscript Received --- 15 Mar. 2021; Revised --- 31 May. 2021; Accepted ---1 Jun. 2021)

Abstract

Nowadays the application of plasma actuators has drawn much attention due to the possibility of creating a volumetric force and, therefore, controlling airflow around rigid bodies. These actuators are among common flow control methods because of availability, lack of need for special repairs, very short response time, and low power consumption. The aim of this study is to reduce the flow separation region and delay the stall angle. Therefore, the airflow over a NACA 0012 airfoil and with a Reynolds number of 1.4×10^6 was simulated using Spalart-Allmaras turbulence model. In the first step, the lift coefficients in the plasma-off mode were investigated at different angles. The stall angle of attack was shown to be 15°. Then, the lift coefficients and the stall angle for different Reynolds numbers were compared. In the second step, the plasma (DBD) actuator was defined using UDF code in Ansys Fluent software as the body force exerted on the airfoil. Plasma activation led to an increase in the lift coefficients at different angles compared to the plasma-off mode. Subsequently, it was shown that the plasma actuator minimizes the flow separation area on the airfoil. Defining this actuator at an optimal position at a constant RE of 1.4×10^6 on a NACA 0012 airfoil where flow separation occurs changed the stall angle of the airfoil from 15° under normal conditions to 19°. The results of the lift coefficient with the help of plasma actuators showed that the airflow on the airfoil is well controlled at sensitive attack angles.

Keywords: Airflow, Electro-hydrodynamics, Plasma (DBD), Flow Separation, Stall Angle.

1- Introduction

A stall angle in aerodynamics or aviation is a condition in which the coefficient of attack begins to decrease if the angle of attack increases from a certain value. The angle at which this begins is called the critical attack angle. The critical angle depends on the cross-section of the airfoil or wing profile, the platform (overview of the aircraft wing from above or below) and the length-to-width ratio, and other factors, but usually varies in the range of 8 to 20 degrees relative to the inlet air for subsonic flows. Stall angle occurs due to the separation of the flow, which itself occurs due to the flow of air in the face of increasing pressure [8, 15]. The Stall angle is a supercritical point, and this study focuses on delaying the flow separation point with aim of DBD actuators, this makes the vortex area smaller and the stall point occurs at higher angles. The

importance of this issue is to provide a new method for the aircraft industry to increase the performance efficiency of an airfoil.

In this study, asymmetric NACA 0012 airfoil is placed at a zero angle of attack (AOA=0) in airflow with a speed of 20 m/s, and the lift coefficient is calculated. The angle of attack is increased in regular steps in the nose-up state, and the lift coefficient is calculated simultaneously. The resulting graph of lift coefficient angle of attack is plotted. At a given angle of attack, the flow must be separated from the airfoil for the stall phenomenon to take place. In this case, the lift coefficient decreases drastically, and the drag coefficient increases. At this moment, the electro-hydrodynamic force is applied, the airflow is reconnected to the cross-section of the airfoil, the lift coefficient is re-calculated, and fly above the stall angle becomes possible. The present study discusses two-dimensional wing aerodynamics; hence, the aspect ratio (AR) is considered unlimited such that three-dimensional effects are eliminated. Stall angle is a supercritical point and must be passed to prevent flow separation. Our aim in this project is to use plasma (DBD) to prevent the lift coefficient from declining at the stall angle and, on the contrary, cause it to increase. This reduces the vortex area and delays flow separation. Among the published articles related to this topic, one can mention the following works. Malik et al. used the jet force derived from a direct flow discharge to create a plasma region and ultimately decrease the drag force on flat plates. Subsequently, numerous researchers used electrical discharge to generate a body force vector, control boundary-layer flow separation, and increase the equal force on different objects [1]. Singh et al. numerically investigated the flow separation phenomenon using plasma actuators on a flat plate having an angle of attack. In this study, they used a self-sustained plasma actuator model to find the electric force field and apply it to the momentum equations. The results of this study showed that applying the body force due to the actuator to the fluid increases the momentum near the wall and eliminates small bubbles inside the flow [2]. Forte et al. investigated the effect of a plasma actuator on airflow over airfoils. They have performed a great deal of research on the effects of geometry, electrode material, input voltage, frequency, and other parameters of the plasma actuator [3]. Also, interesting and applied research works have been carried out about plasma technologies [4-6]. In addition, as an important, applied and different research in the plasma field, Ramirez et al. [7], recently analyzed plasma membrane V-ATPase controls oncogenic RAS-induced micropinocytosis in NATURE and also, applied and interesting research works have been done about airflow analysis [20–30]. In the present research, we intend to use a plasma actuator at a Reynolds number of 1.4×10^6, the Spallart-Almaras turbulence model, and the Ansys Fluent software to make the flight occur at the stall angle, i.e., to delay stall using electro-hydrodynamic actuators.

2- Methods

This study attempts to study the flow around the airfoil, NACA 0012 airfoil geometry, modeling and meshing of the geometry, and the effects related to plasma actuators. For this purpose, an airfoil is considered in the flow regime and its momentum, continuity, and turbulence equations are solved numerically.

The goal here is to examine the flow near an airfoil. To this end, the computational

domain must first be drawn. Then, the domain must have meshed, and the boundary conditions must be specified. Finally, the results must be derived after solving the equations numerically.

2-1- Computation space and meshing

Fig.1 presents a computational domain along with meshing that includes boundary conditions, namely flow inlet, flow outlet, and airfoil wall. As can be seen, a finer mesh is used near the airfoil, as the computational accuracy in these areas should be greater.

2-2- Boundary conditions

In this study, a Reynolds number of 1.4×10^6 is assumed for the flow around the airfoil, as can be calculated from Eq. (1) [8].

$$Re = \frac{\rho v C}{\mu} \quad (1)$$

where ρ is the air density, v is the velocity of the flow, c is the chord length of the airfoil and μ is the dynamic viscosity of the air. Also, the problem definition and flow simulation method using Ansys Fluent software are as follows. The reference parameters in this research are as in Table 1. Also, the input data for simulation in Ansys Fluent software are presented in Table 2.

2-3 Equations

In this study, the attempt is to study the flow around an airfoil and to investigate the plasma actuator effects. For this purpose, an airfoil is considered in the flow regime, and the equations of momentum, continuity, and turbulence are solved numerically.

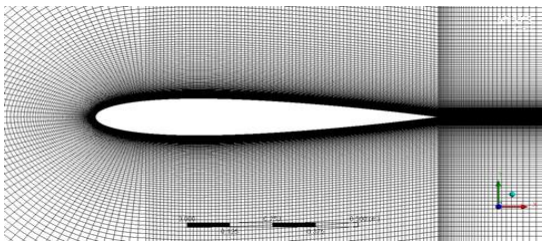

Fig. 1 Meshing near the NACA0012 airfoil.

Table 1: Reference Parameters.

Parameter	Value	Symbol	Unit
Reynolds number	-	*Re*	-
Air density	1.225	ρ	$\boldsymbol{kg/m^3}$
dynamic viscosity	1.7894×10^{-5}	μ	*kg / m.s*
Airfoil chord length	1	*C*	*m*
Flow velocity	20	*V*	*m/s*

Table 2: Input data for simulation in Ansys Fluent software

Computational domain	2D
Time dependence	Steady
Turbulence model	*Spalart-Allmaras*
Turbulence viscosity ratio	10
Temperature	300 K
Pressure	101325 Pa

2-3-1 Continuity Equation

The continuity equation states that if we place a control volume in a fluid region, the inlet and outlet mass flows are equal when there is no generation of mass. Below is the continuity equation in this case [8].

$$\frac{\partial}{\partial x}(\rho u) + \frac{\partial}{\partial y}(\rho v) + \frac{\partial}{\partial z}(\rho w) = 0 \quad (2)$$

As shown above, the continuum equation is for a three-dimensional flow state. However, since this case two-dimensional, the above equation is simplified as follows.

$$\frac{\partial}{\partial x}(\rho u)+\frac{\partial}{\partial y}(\rho v)=0 \quad (3)$$

2-3-2 Momentum Equations

The Navier–Stokes equations or the fluid motion equations are derived from Newton's second law, which is the principle of conservation of momentum [8],

$$\frac{\partial u}{\partial t}+u\frac{\partial u}{\partial x}+v\frac{\partial u}{\partial y}+\frac{1}{\rho}\frac{\partial}{\partial y}\left(\mu\frac{\partial u}{\partial y}\right) = -\frac{1}{\rho}\frac{\partial p}{\partial x}+\frac{1}{\rho}\frac{\partial}{\partial x}\left(\mu\frac{\partial u}{\partial x}\right) - \left(\frac{\mu}{\alpha}v_i+c_2\frac{1}{2}\rho|v|v_i\right) \quad (4a)$$

$$\frac{\partial v}{\partial t}+u\frac{\partial v}{\partial x}+v\frac{\partial v}{\partial y}=-\frac{1}{\rho}\frac{\partial p}{\partial y}+ \frac{1}{\rho}\frac{\partial}{\partial x}\left(\mu\frac{\partial v}{\partial x}\right)+\frac{1}{\rho}\frac{\partial}{\partial y}\left(\mu\frac{\partial v}{\partial y}\right) - \left(\frac{\mu}{\alpha}v_i+c_2\frac{1}{2}\rho|v|v_i\right) \quad (4b)$$

These equations are obtained with the following assumptions,

• Non-steady fluid flow

• Constant thermal and physical properties of the fluid with respect to temperature

• Absence of external and body forces

• Two-dimensional fluid flow

It is further noted that heat transfer and hydrodynamics are being considered in a time-independent manner. Therefore, the above equations are modified and expressed as follows [8],

$$u\frac{\partial u}{\partial x}+v\frac{\partial u}{\partial y}=-\frac{1}{\rho}\frac{\partial p}{\partial x}+\frac{1}{\rho}\frac{\partial}{\partial x}\left(\mu\frac{\partial u}{\partial x}\right)+\frac{1}{\rho}\frac{\partial}{\partial y}\left(\mu\frac{\partial u}{\partial y}\right)-\left(\frac{\mu}{\alpha}v_i+c_2\frac{1}{2}\rho|v|v_i\right) \quad (5)$$

$$u\frac{\partial v}{\partial x}+v\frac{\partial v}{\partial y}=-\frac{1}{\rho}\frac{\partial p}{\partial y}+\frac{1}{\rho}\frac{\partial}{\partial x}\left(\mu\frac{\partial v}{\partial x}\right)+\frac{1}{\rho}\frac{\partial}{\partial y}\left(\mu\frac{\partial v}{\partial y}\right)-\left(\frac{\mu}{\alpha}v_i+c_2\frac{1}{2}\rho\left|v|v_i\right.\right) \quad (6)$$

2-3-3 Spalart-Allmaras turbulence model

The model is designed for aerodynamic flow, including transonic flows over the airfoil, where boundary layer separation is involved [16, 17]. The model equation is of the form [18, 19],

$$\frac{D\tilde{v}}{Dt}=c_{b1}[1-f_{t2}]\tilde{S}\tilde{v}+\frac{1}{\sigma}\left[\nabla.\left((v+\tilde{v})\nabla\tilde{v}\right)c_{b2}(\nabla\tilde{v})^2\right]-\left[c_{w1}f_w-\frac{c_{b1}}{k^2}f_{t2}\right]\left[\frac{\tilde{v}}{d}\right]^2+f_{t1}\,\Delta U^2 \quad (7)$$

where v is the molecular viscosity. The individual components of the production term are defined as,

$$\tilde{S}\equiv S+\frac{\tilde{v}}{k^2d^2}\left[-\left(\frac{\tilde{v}}{v}\right)\left[+\frac{\left(\frac{\tilde{v}}{v}\right)^4}{\left[\left(\frac{\tilde{v}}{v}\right)^3+C_{v1}^3\right]}\right]^{-1}\right] \quad (8)$$

where d is the distance to the closet wall, and S is the magnitude of the vorticity. The function f_w is written as follows,

$$\begin{cases} f_w=g\left[\dfrac{1+C_{w3}^6}{g^6+C_{W3}^6}\right]^{\frac{1}{6}} \\ g=r+C_{w2}(r^6-r) \\ r\equiv\dfrac{\tilde{v}}{\tilde{S}k^2d^2} \end{cases}$$

The functions $f_{t1}\ and\ f_{t2}$ are as

$$f_{t1}=C_{t1}g_t\exp\left(-C_{t2}\frac{\omega_t^2}{\Delta U^2}[d^2+g_t^2d_t^2]\right) \quad (9)$$

$$f_{t2}=C_{t3}\exp[-C_{t4}(\tilde{v}/v)^2] \quad (10)$$

where d_t is the distance from the point in the flow field to the trip on the wall, ΔU is the difference between velocity at the field point and that at the trip, w_t is the wall vorticity at the trip, and $g_t=\min(0.1,\Delta U/$

$\omega_t \Delta x_t$) , where is the grid spacing along the wall at the trip [18, 19].

2-3-4 Electro-hydrodynamic force equation

The continuity equation for each element i in the plasma is obtained from the Boltzmann equation, as in Eq. (11) [9-11].

$$\frac{\partial n_i}{\partial t} + \nabla . \Gamma_i = S_i \quad (11)$$

In this equation n_i is the density of the element *i*, F_i is the flux of *i*, and S_i is a source term that shows the rate of change of density of *i* caused by chemical reactions and is calculated as in Eq. (12) [9-11].

$$s_i = \sum_r C_{i,r} R_{i,r} = \sum_r \left[C_{i,r} K_r \prod_j n_j \right] \quad (12)$$

In Eq. (12) *r* is the subscript for production or dissipation reaction for *i*, $c_{i,r}$ is the stoichiometric coefficient of i in reaction *r*, $R_{i.r}$ is the reaction rate, K_r is reaction rate coefficient, and the subscript j is related to the reacting elements. In Eq. (11) the drift-diffusion approximation is used to calculate the flux. Considering the effects of ambient fluid velocity, the flux relationships for electrons, ion elements, and neutral elements are obtained from Eqs (13)-(15), respectively [9-11].

$$\vec{\Gamma}_e = -\mu_e n_e \vec{E} - D_e \vec{\nabla} n_e + n_e \vec{V} \quad (13)$$

$$\vec{\Gamma}_i = -\mu_i n_i \vec{E} - D_i \vec{\nabla} n_i + n_i \vec{V} \quad (14)$$

$$\vec{\Gamma}_{uc} = -D_{uc} \vec{\nabla} n_{uc} + n_{uc} \vec{V} \quad (15)$$

In the above relationships $\vec{E}$ is the electric field, μ_i is the electrical excitability and D_i is the diffusion coefficient for element *i*. The mobility and diffusion coefficients are determined by the interactions between the elements and the background gas according to the following equations [9-11].

$$\mu_i = \frac{q_i}{m_i v_i} \quad (16)$$

$$D_i = \frac{k_B T_i}{m_i v_i} \quad (17)$$

In the above equations, q_i is the electric charge of element *i*, m_i is the mass of element *i*, v_i is the frequency of momentum collision between element *i* and the background gas, k_b is the Boltzmann constant, and T_i is the temperature of element *i*. Heavy particles are assumed to be in thermal equilibrium with the background gas; therefore, there is no need to solve the energy equation for these particles, and the energy relation is solved for electrons only. This relation for electrons is in the form of Eq. (18) [9-11].

$$\frac{\partial n_\varepsilon}{\partial t} + \nabla . \Gamma_\varepsilon = S_\varepsilon \quad (18)$$

In this relationship, n_ε is the density of electron energy, defined as $n_\varepsilon = n_e \bar{\varepsilon}$, and $\bar{\varepsilon}$ is the average energy of electrons, which is associated with the temperature of electrons through Eq. (19) [9-11].

$$k_b T_e = \frac{2\bar{\varepsilon}}{3} \quad (19)$$

Also, the electron energy flux can be calculated from Eq. (20) [9-11].

$$\vec{\Gamma}_\varepsilon = -\frac{5}{3} \mu_e n_\varepsilon \vec{E} - \frac{5}{3} D_e \vec{\nabla} n_\varepsilon + n_\varepsilon \vec{v} \quad (20)$$

The source term in the energy equation is derived from Eq. (21). The additional part of this term is due to the Ohmic heating of the electron by the electric field [9-11].

$$S_\varepsilon = -e\Gamma_e . E - n_e \sum_r \bar{\varepsilon}_r K_r n_r \quad (21)$$

The two terms on the right side represent the heat generated by the electric field and the electron energy loss due to collisions, respectively. The parameter *"r"* denotes the reactions leading to electron collisions. The parameter *"*n_r" is the density of the target element, and *"*$\bar{\varepsilon}_r$*"* is the reaction threshold energy. Using the Gauss law, the

electric field is related to the charge density through Eq. (20) [9-11].

$$\nabla.(\epsilon E) = -\nabla.(\epsilon\nabla\phi) = \rho_c \quad (22)$$

The charge density can be calculated as follows.

$$\rho_c = \sum_i q_i n_i \quad (23)$$

Finally, the electro-hydrodynamic force applied to the fluid due to the electric field and the charged particles in the fluid can be calculated by means of Eq. (24) [9-11].

$$\vec{F}_{EHD} = \rho_c \vec{E} = -\nabla\Phi \sum_i q_i n_i \quad (24)$$

2-4 Navier-Stokes plasma equation

For fluid flow, the continuity equation (23) and momentum equation (24) are solved in *x* and *y* directions, and since in non-thermal plasma, the gas temperature remains at ambient temperature, there is no need to solve the energy equation for the fluid. In this equation, ρ and *v* are the density and the velocity vector, respectively.

$$\frac{\partial\rho}{\partial t} + \nabla.(\rho V) = 0 \quad (25)$$

The momentum equation for the incompressible state, known as the Navier-Stokes equation, is expressed as in Eq. (26).

$$\rho\left(\frac{\partial v}{\partial t} + v.\nabla v\right) = -\nabla p + \mu\nabla^2 v + F_{EHD} \quad (26)$$

In this relationship, "P" is the pressure, "μ" is the dynamic viscosity of the fluid, and "F_{EHD}" is the body force caused by the plasma phenomenon (per unit volume) [11].

3- Results and discussion

In this section, several topics are discussed, and the results for each variable are evaluated, as follows:

- Examining the flow around NACA 0012 airfoil in plasma-off and plasma-on modes
- Investigating and calculating the lift coefficients according to the angles of attack of 5, 10, 12, 14, 15, 16, 17, 18, 19 degrees in the plasma-off and plasma-on modes
- Calculating the stall angle in the plasma-off mode
- Delaying the critical stall angle

3-1 Investigating the velocity contour (plasma-off)

In this part of the study, the velocity contours at angles of 10°, 15°, 18° were simulated using the Spalart-Allmaras turbulence model. According to Figs. 2(a)-(c), a smaller flow separation has occurred at an angle of 10° compared to 15° and 18°. As the angle of attack increases, the vortices and return flows have increased in the separation zone at an angle of 15°, and they reach their maximum at an angle of 18°.

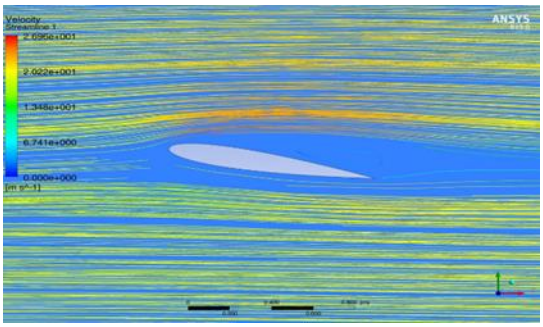

(a)

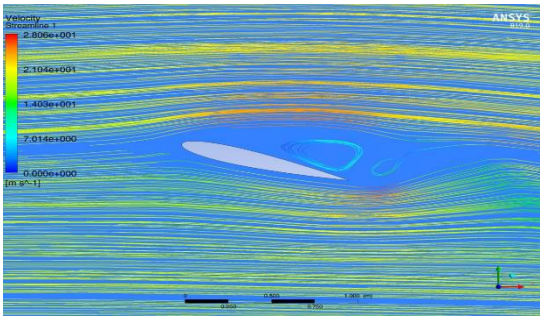

(b)

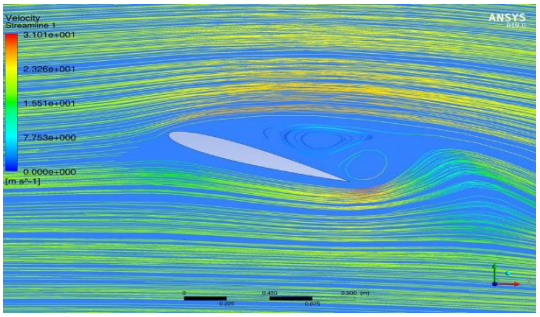

(c)

Fig. 2 **(a)** Flow velocity contour at angle of attack of 10° (plasma-off), **(b)** Flow velocity contour at angle of attack of 15° (plasma-off), **(c)** Flow velocity contour at angle of attack of 18° (plasma-off).

3-2 Investigating the velocity contour (plasma on)

In Figs. 3(a)-(c), direct flow and the angles of attack of 10°, 15°, and 18° on the airfoil are shown for the plasma on mode. In this case, the absence of flow separation is evident. The plasma has also minimized the vortices and return flows at these angles and the flow is connected to the airfoil cross section. According to the results, in the plasma-on mode, the velocity at the airfoil surface significantly increases. as well as the lift coefficient increase. It can be concluded that plasma functions have a positive effect on controlling the flow over an airplane.

3-3 Examination of lift coefficients and stall angle

The stall area, or stall angle, is a supercritical area where the flow is separated from the airfoil at an angle of attack, leading to the stall phenomenon and the crashing of the plane [8, 22].

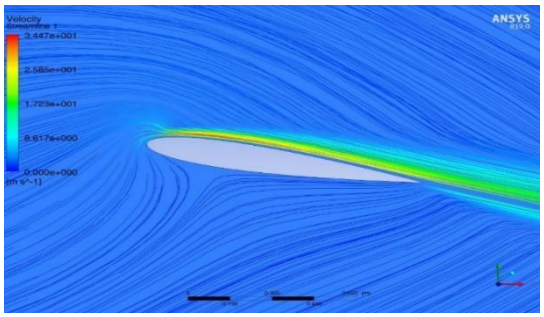

(a)

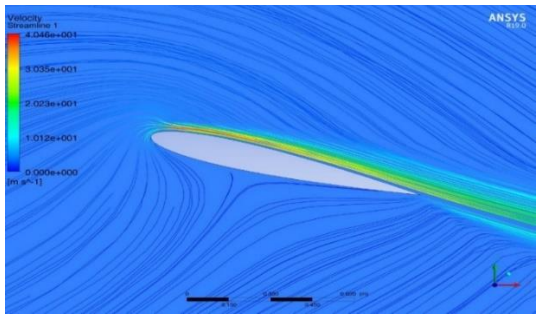

(b)

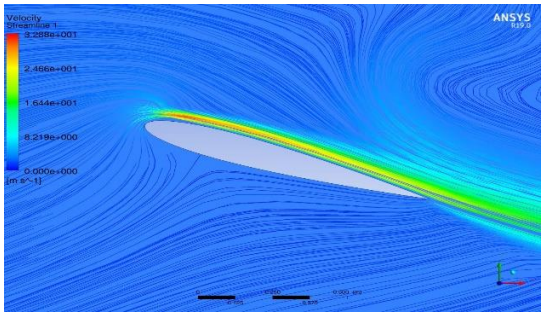

(c)

Fig. 3 **(a)** Flow velocity contour at an angle of attack of 10° (plasma on), **(b)** Flow velocity contour at an angle of attack of 15° (plasma on), **(c)** Flow velocity contour at an angle of attack of 18° (plasma on).

The stall angle is different for different Reynolds numbers.

In this study, for the purpose of comparison and verification, lift coefficients plotted against angle of attack for NACA 0012 by Critzos et al. [12], Winslow et al. [13] as well as numerical results from Malhotra et al. [14] have been used to show where stall occurs at different Reynolds numbers. To determine the lift coefficient points, the angles of attack of $5^{\circ}, 10^{\circ}, 12^{\circ}, 14^{\circ}, 15^{\circ}, 16^{\circ}, 17^{\circ}, 18^{\circ}, 19^{\circ}$ are

calculated for a Reynolds number of 1.4×10^6 in plasma off and plasma on modes.

To precisely determine this critical point, the angle of attack has been increased incrementally at an angle of 14 °, with regular increments of one degree. In Fig. 4(a), the stall point is examined in Plasma-off and Plasma-on modes. The results obtained for the lift coefficient in the plasma-off mode are compared with the laboratory results by Critzos et al., the numerical results by Malhotra et al., and the numerical results by Winslow et al. Critzos et al. experimentally examined the aerodynamic characteristics of the NACA 0012 airfoil at a Reynolds number of 5×10^5 at angles of attack of 0 to 180 degrees. Malhotra et al. have investigated the stall angle and numerical simulation of turbulent flow at a Reynolds number of 3×10^6. Winslow et al. have numerically investigated the lift and drag coefficients at different angles of attack and different Reynolds numbers on 0009 and 0012 airfoils. In Fig. 4(a), the results of these solutions compared with each other. As can be seen, in the laboratory values of Critzos et al., at the Reynolds number of 5×10^5, the highest lift coefficient was at the angle of attack of 12 °, after which it decreased. In the numerical solution of Malhotra et al., at the Reynolds number of 3×10^6, the highest lift coefficient and stall angle were at an angle of attack 16 °. Moreover, in the numerical results of Winslow et al., at a Reynolds number of 1×10^6, the highest lift coefficient was at the angle of attack of 14°, which represented the critical point. In this study, the highest lift coefficient and stall angle were calculated at a Re of 1.4×10^6 and angle of attack of 15 °.

At high Reynolds numbers, the stall angle of Airfoil NACA 0012 was around an angle of attack of 15° [15].

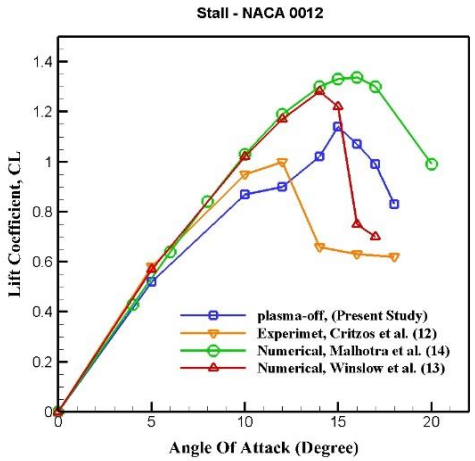

(a)

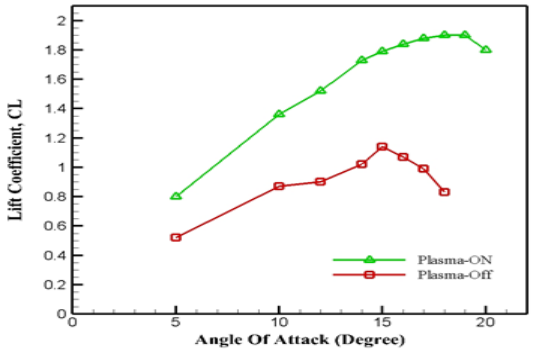

(b)

Fig. 4 **(a)** Lift coefficient versus angle of attack in the plasma-off mode compared with the experimental results of Critzos et al. [12], the numerical results of J. Winslow et al [13], and the numerical results of Malhotra et al. [14] **(b)** Results of lift coefficients in terms of angle of attack in Plasma-off and Plasma-on modes.

After examining the lift coefficient in plasma off mode with the experimental values of Critzos et al., the numerical results of Malhotra et al., and the numerical results of Winslow et al, we now intend to investigate the lift coefficient, using Fig. 4(b), in plasma off and plasma on modes. As shown in Fig. 4 in the plasma off mode, as the angle of attack increases, the lift coefficient reaches its maximum value at 15°. Then, the lift coefficient drops sharply

at the angles of attack of 16°, 17°, 18°, 19°. Angles above 16° in the plasma off mode are supercritical angles. As shown in Fig. 4(b), the stall point has occurred at a Reynolds number of 1.4×10^6 and an angle of attack of 15°. it is observed in the figure in the plasma on mode that the lift coefficient has not decreased at the angle of attack of 15°. This indicates that the plane does not crash at the stall angle with the aid of plasma. According to Fig. 4(b), with plasma activation, the lift coefficient results at angles of attack of 18 ° and 19° are 1.90175 and 1.90177, respectively. In other words, these supercritical angles are well controlled with the help of plasma. After calculating the lift coefficient at an angle of attack of 20°, the lift coefficient decreased from 1.90 to 1.80. As shown in the figure, when plasma is active, the stall angle occurs at an angle of attack of 19°.

4- Conclusion

The overall results of this research are as follows,

- In the plasma off mode, with increasing angle of attack, the flow separation area increase, and vortices are created behind the airfoil. With the addition of plasma, the separation zone decreases at large angles of attack and the return flows or vortices behind the airfoil are minimized which causes the control of the airflow over the airfoil is greatly improved, making it easier for the pilot to fly the airplane.
- In plasma on mode, the lift coefficient results at angles of attack of 18° and 19° were 1.90175 and 1.90177, respectively, indicating that the lift coefficient has not reduced at an angle of attack of 19° and the flow on the airfoil has been controlled at this supercritical angle. However, at the angle of attack of 20 °, the lift coefficient fell from 1.90 to 1.80. Inactive plasma mode, the stall angle of the NACA 0012 airfoil is 19°.
- Applying this actuator at an optimum position on the NACA 0012 airfoil, where the flow separates, and at the constant Reynolds number of 1.4×10^6 reduced the airfoil stall angle from 15° under normal conditions to 19°.
- The results of the lift coefficients when the plasma actuators are active show that the stall point is delayed and the flow separation does not occur at sensitive attack angles, making it easy for the pilot.

Finally, it is suggested that the flow and pressure on the airfoil can be controlled with the aid of plasma by applying 2 or 3 plasmas in different parts of the airfoil.

References

[1] Malik, M., Weinstein, L., & Hussaini, M. (1983, January). Ion wind drag reduction. In *21st Aerospace Sciences Meeting* (p. 231).

[2] Singh, K. P., Roy, S., & Gaitonde, D. V. (2006). Study of control parameters for separation mitigation using an asymmetric single dielectric barrier plasma actuator. *Plasma Sources Science and Technology*, *15*(4), 735.

[3] Forte, M., Jolibois, J., Pons, J., Moreau, E., Touchard, G., & Cazalens, M. (2007). Optimization of a dielectric barrier discharge actuator by stationary and non-stationary measurements of the induced flow velocity: application to airflow control. *Experiments in fluids*, *43*(6), 917-928.

[4] Vlad, M., & Spineanu, F. (2015). Evolution of plasma turbulence beyond the quasilinear regime; a semi-analytical study. *Romanian Reports in Physics*, *67*(3), 1074-1086.

[5] Diplasu, C., Giubega, G., Ungureanu, R., Cojocaru, G., Serbanescu, M., Marcu, A., & Zamfirescu, M. (2021). Commissioning experiment on laser-plasma electron acceleration in supersonic gas jet at cetal-pw laser facility. *Romanian Reports in Physics*, *73*, 401.

[6] Šerá, B., Vanková, R., Roháček, K., & Šerý, M. (2021). Gliding Arc Plasma Treatment of Maize (Zea mays L.) Grains Promotes Seed Germination and Early Growth, Affecting Hormone Pools, but Not Significantly Photosynthetic Parameters. *Agronomy*, *11*(10), 2066.

[7] Ramirez, C., Hauser, A. D., Vucic, E. A., & Bar-Sagi, D. (2019). Plasma membrane V-ATPase controls oncogenic RAS-induced macropinocytosis. *Nature*, *576*(7787), 477-481.

[8] Anderson Jr, J. D. (2010). *Fundamentals of aerodynamics*. Tata McGraw-Hill Education.

[9] Castellanos, A. (Ed.). (1998). *Electrohydrodynamics* (Vol. 380). Springer Science & Business Media..

[10] Nagaraja, S., Yang, V., & Adamovich, I. (2013). Multi-scale modelling of pulsed nanosecond dielectric barrier plasma discharges in plane-to-plane geometry. *Journal of Physics D: Applied Physics*, *46*(15), 155205.

[11] Babou, Y., Martin, E. N., & Peña, P. F. (2017, July). Simple body force model for Dielectric Barrier Discharge plasma actuator. In *Proceedings of the 7th European Conference for Aeronautics and Aerospace Sciences (EUCASS), Milan, Italy* (pp. 3-6).

[12] Critzos, C. C., Heyson, H. H., & Boswinkle, R. W. (1955). Aerodynamic characteristics of NACA 0012 airfoil section at angles of attack from 0 to 180 degrees. National Advisory Committee for Aeronautics.

[13] Winslow, J., Otsuka, H., Govindarajan, B., & Chopra, I. (2018). Basic understanding of airfoil characteristics at low Reynolds numbers (10 4–10 5). Journal of Aircraft, 55(3), 1050-1061.

[14] Malhotra, A., Gupta, A., & Kumar, P. (2017). Study of static stall characteristics of a NACA 0012 aerofoil using turbulence modeling. In *Innovative Design and Development Practices in Aerospace and Automotive Engineering* (pp. 369-378). Springer, Singapore.

[15] Barnard, R. H., & Philpott, D. R. (2010). *Aircraft flight: a description of the physical principles of aircraft flight*. Pearson education.

[16] Pope, S. B., & Pope, S. B. (2000). *Turbulent flows*. Cambridge university press.

[17] Mathieu, J. M., & Scott, J. F. (2000). *Turbulent flows*.

[18] Eleni, D. C., Athanasios, T. I., & Dionissios, M. P. (2012). Evaluation of the turbulence models for the simulation of the flow over a National Advisory Committee for Aeronautics (NACA) 0012 airfoil. *Journal of Mechanical Engineering Research*, *4*(3), 100-111.

[19] Spalart, P., & Allmaras, S. (1992, January). A one-equation turbulence model for aerodynamic flows. In *30th aerospace sciences meeting and exhibit* (p. 439).

[20] Alipour, H., Karimipour, A., Safaei, M. R., Semiromi, D. T., & Akbari, O. A. (2017). Influence of T-semi attached rib on turbulent flow and heat transfer parameters of a silver-water nanofluid with different volume fractions in a three-dimensional trapezoidal microchannel. *Physica E: Low-Dimensional Systems and Nanostructures*, *88*, 60-76.

[21] Akbari, O. A., Toghraie, D., & Karimipour, A. (2016). Numerical simulation of heat transfer and turbulent flow of water nanofluids copper oxide in rectangular microchannel with semi-attached rib. *Advances in Mechanical Engineering*, *8*(4), 1687814016641016.

[22] Rezaei, O., Akbari, O. A., Marzban, A., Toghraie, D., Pourfattah, F., & Mashayekhi, R. (2017). The numerical investigation of heat transfer and pressure drop of turbulent flow in a triangular microchannel. *Physica E: Low-dimensional Systems and Nanostructures*, *93*, 179-189.

[23] Pourfattah, F., Motamedian, M., Sheikhzadeh, G., Toghraie, D., & Akbari, O. A. (2017). The numerical investigation of angle of attack of inclined rectangular rib on the turbulent heat transfer of Water-Al2O3 nanofluid in a tube. *International Journal of Mechanical Sciences*, *131*, 1106-1116.

[24] Parsaiemehr, M., Pourfattah, F., Akbari, O. A., Toghraie, D., & Sheikhzadeh, G. (2018). Turbulent flow and heat transfer of Water/Al2O3 nanofluid inside a rectangular ribbed channel. *Physica E: Low-Dimensional Systems and Nanostructures*, *96*, 73-84.

[25] Hosseinnezhad, R., Akbari, O. A., Afrouzi, H. H., Biglarian, M., Koveiti, A., & Toghraie, D. (2018). Numerical study of turbulent nanofluid heat transfer in a tubular heat exchanger with twin twisted-tape inserts. *Journal of Thermal Analysis and Calorimetry*, *132*(1), 741-759.

[26] Toghraie, D. (2016). Numerical thermal analysis of water's boiling heat transfer based on a turbulent jet impingement on heated surface. *Physica E: Low-Dimensional Systems and Nanostructures*, *84*, 454-465.

[27] Pourdel, H., Afrouzi, H. H., Akbari, O. A., Miansari, M., Toghraie, D., Marzban, A., & Koveiti, A. (2019). Numerical investigation of turbulent flow and heat transfer in flat tube. *Journal of Thermal Analysis and Calorimetry*, *135*(6), 3471-3483.

[28] Bigdeli, M., & Monfared, V. (2020). Investigation and comparison of stall angle of airfoil naca 0012 in reynolds number of 3× 106 with k-ω sst, realizable k-ε, spalart-allmaras turbulence models. *Comptes rendus de l'Académie bulgare des Sciences*, *73*(3).

[29] Bigdeli, M., Mohammadi, R., Bigdeli, J., & Monfared, V. (2021). Study on drag coefficient via dielectric barrier discharge (DBD) plasma actuators. *Digest Journal of Nanomaterials & Biostructures (DJNB)*, *16*(2).

[30] Monfared, V., Tathiri, G., Ansari, A., & Bigdeli, M. (2020). Reducing the Airflow Separation Region and Turbulence around the Airfoil using a Body Force. *Journal of Mechanical Research and Application*, *10*(2), 34-47.